Satellite-Based Precipitation Measurement Using PERSIANN System

Kuo-Lin Hsu and Soroosh Sorooshian

Abstract PERSIANN (Precipitation Estimation from Remotely Sensed Information using Artificial Neural Networks) is a satellite-based rainfall estimation algorithm. It uses local cloud textures from longwave infrared images of the geostationary environmental satellites to estimate surface rainfall rates based on an artificial neural network algorithm. Model parameters are frequently updated from rainfall estimates provided by low-orbital passive microwave rainfall estimates. The PERSIANN algorithm has been evolving since 2000, and has generated near real-time rainfall estimates continuously for global water and energy studies. This paper presents the development of the PERSIANN algorithm in the past 10 years. In addition, the validation and merging PERSIANN rainfall with ground-based rainfall measurements for hydrologic applications are also discussed.

Keywords PERSIANN · Artificial neural network · Precipitation · Precipitation data merging

1 Introduction

Realistic precipitation estimation is crucial to the global climate and land surface hydrologic studies. However, while rain gauges and radar can provide relatively continuous measurements with high temporal frequency, the gauges are sparsely located and provide only point-scale measurements and the radar coverage is limited by topography. The limitation of in-situ precipitation observation over the remote regions makes global climatic and hydrological studies rely mainly on satellite observations and the numerical weather prediction modeling analysis.

Since the 1970s, the satellite information has been used to analyze precipitation. Since then, a large number of rain retrieval algorithms have been developed. As visible (VIS) and infrared (IR) images provide excellent temporal resolutions of

K.-L. Hsu
Center of Hydrometeorology and Remote Sensing (CHRS), Department of Civil and Environmental Engineering, University of California, Irvine

S. Sorooshian et al. (eds.), *Hydrological Modelling and the Water Cycle*, 27–48

cloud albedo and top temperatures less than an hour from geosynchronous orbit (GEO) satellites; they are frequently used to monitor cloud motion. These image channels, however, do not provide direct information to infer the actual rainfall at the ground surface. The indirect relationship gives rise to the retrieval of surface rainfall with high uncertainty.

Passive Microwave (PMW) sensors carried by satellites in low earth orbits (LEO) sense rainfall clouds more directly. The rain retrieval algorithms based on PMW sensors provide better instantaneous rainfall estimate, however the hind side is that, each LEO satellite only provides limited (1–2) samples in a day for a specified study area.

In 1997, the launch of the Tropical Rainfall Measurement Mission (TRMM) provided the first satellite to measure precipitation with an orbital radar sensor to calibrate the other passive microwave sensors (Kummerow et al., 1998; Kummerow et al., 2000; Simpson et al., 1988). Because of its superior sensor and non-sun synchronous orbit, TRMM data are regularly used to calibrate and integrate information from other satellite-based rainfall measurements (NRC report, 2004). The follow on mission of TRMM, the Global Precipitation Measurement (GPM), is in the planning stage. With enhanced dual frequency radar sensors and deployment of a constellation of pre-existing and new experimental satellites with microwave sensors on board, the deployment of Global Precipitation Mission (GPM) satellites will cover more than 90% of the globe sampled within a return interval of less than 3-hours (Hou, 2006).

To overcome the less frequent sampling problem, by effective integration of information from several satellites, a better spatial/temporal coverage of diurnal rainfall pattern as well as continuous monitoring of heavy storm events may be obtained. To utilize both the strengths and compensate the weaknesses of those PMW and IR sensors, algorithms were developed to jointly use GEO and LEO satellite information. The results demonstrated the great potential of improving surface rainfall retrieval (Adler et al., 1993; Ba and Gruber, 2001; Bellerby et al., 2000; Hsu et al., 1997, 1999; Huffman et al., 1997, 2001; Lavizzani et al., 2007; Marzano et al., 2004; Miller et al., 2001; Sorooshian et al., 2000; Tapiador et al., 2004a; Turk et al., 2000; Vicente et al., 1998; Xie and Arkin, 1997; Xu et al., 1999). Validation of satellite-based precipitation products has been established in the past 15 years (Arkin and Xie, 1994; Xie and Arkin, 1995; Ebert and Manton, 1998; Adler et al., 2001; Xie et al., 2003). The results have shown that the combined multiple satellite sensors offer superior results (Ebert et al., 2006; Turk et al., 2006).

Following this progress, many satellite-based high resolution precipitation products have been in routine operation for generating near real-time global coverage of precipitation (Huffman et al., 2002; Turk et al., 2000; Joyce et al., 2004; Vicente et al., 1998; Tapiador et al., 2004a; Sorooshian et al., 2000; Hong et al., 2004). A recent validation activity, the Pilot Evaluation of High Resolution Precipitation Products (PEHRPP) program, sponsored by the International Precipitation Working Group (IPWG), plans to evaluate the high-resolution precipitation products (Arkin et al., 2005). The evaluation regions of HRPP include Australia, United States, and Europe and will be extended to other regions, such as Japan, Korea, Taiwan, etc. The

evaluation focuses on the large-scale validation of daily rainfall estimates at higher spatial and temporal resolutions.

In addition to satellites, precipitation observations are also available from many other sources, such as radar and gauges. These sources differ significantly in their sampling scale and resolution, as well as the information content to interpret the surface rainfall. Because each measurement technically has its own strengths and weakness, suitable integration of those sensors may provide better measurement than one single sensor alone. The challenge has been the development of systematic measurements of global precipitation using multiple satellites, and the effective merging of precipitation data from many other sources, including gauge, radar, and satellite observations.

This paper describes the precipitation estimation using data fusion methods to integrate precipitation observations from several data sources. The contents cover several activities, including: (1) the development and operation of the Precipitation Estimation from Remotely Sensed Information using Artificial Neural networks (PERSIANN), a multiple satellite-based precipitation estimation algorithm; this algorithm integrates the local texture of the GEO IR image and LEO PMW rainfall rates to generate near global precipitation estimates; (2) the extension of IR pixel-based in the original PERSIANN algorithm to cloud patch-based classification methods leads to the development of the PERSIANN Cloud-patch Classification System (PERSIANN-CCS). This algorithm includes more effective IR cloud-patch texture information to the rainfall retrieval; (3) approaches to reduce the PERSIANN product bias and quantify the random error of merged product using satellite and ground based observations; and (4) evaluation and application of satellite-based PERSIANN rainfall estimates. A summary is given in the final section.

2 Precipitation Estimation from Remotely Sensed Information Using Artificial Neural Networks (PERSIANN)

Artificial Neural Network (ANN) models, being well known for their flexibility and capability of modeling complex nonlinear processes, are widely applied in the forecasting and control of nonlinear systems. The applications of ANNs have been extended to the modeling of hydrologic and environmental systems in the 1990s (ASCE Task Committee, 2000; Govindaraju and Rao, 2000; Maier and Dandy, 2000; Krasnopolsky and Schiller, 2003; Krasnopolsky and Chevallier, 2003). As for rainfall estimation from satellite imagery, many algorithms based on ANNs have been developed and are continuously being improved (Bellerby et al., 2000; Coppola et al., 2006; Grimes et al., 2003; Hong et al., 2004; Hsu et al., 1997; Tapiador et al., 2004a,b).

The development of the Precipitation Estimation from Remotely Sensed Information using Artificial Neural Networks (PERSIANN) is based on the more reliable but less frequently sampled instantaneous precipitation rate from microwave sensors to adjust the mapping function of the infrared image of GEO satellites and rainfall

rate. The input features of PERSIANN are extracted from the local image texture of the longwave IR imagery (10.2–11.2 μ m) of GEO satellites. The mapping function of ANN using longwave (10.2–11.2 μm) IR image to the rainfall map is implemented by (1) extracting the local image texture, in terms of calculating the mean and variance of IR brightness temperature near the calculation pixel, (2) classifying the extracted feature, and (3) multivariate mapping of classified texture to the surface rainfall rate. An adaptive training feature facilitates updating of the network parameters whenever independent estimates of rainfall are available (Hsu et al., 1997; Sorooshian et al., 2000). The parameters of PERSIANN are constantly updated when PMW-based rainfalls are available (Ferraro and Marks, 1995; Hsu et al., 1997; Janowiak et al., 2001). The system first used GEO IR imagery. It was later extended to use both GEO IR and VIS imagery and found that the rainfall estimates were improved (Hsu et al., 1999). The PERSIANN algorithm estimates rainfall rate at each $0.25^\circ \times 0.25^\circ$ pixel of every 30 minutes. The estimated rainfall is then integrated to various spatial and temporal scales, such as six-hour, daily, monthly, etc.

In the operation of PERSIANN, two PERSIANN algorithms are running in parallel: one is run in the simulation mode and the other in the update mode. The simulation mode generates the surface rain rate at the $0.25^\circ \times 0.25^\circ$ resolution at every 30 minutes from the GEO satellites infrared images, while the update mode continuously adjusts the mapping function parameters of PERSIANN based on the fitting error of any pixel for which a PMW instantaneous rainfall estimate is available. The simulation mode generates the regular rainfall rate output, and the update mode improves the quality of the product. The accuracy of the final product, however, depends on many factors, such as the effectiveness of the input feature detection and classification scheme, the accuracy of the individual input-output mapping functions, and the accuracy and frequency of the PMW rainfall estimates used for updating (Sorooshian et al., 2000). Description of the current operation of PERSIANN is listed in Fig. 1. IR imagery is provided by GEO satellites, such as GOES-8, GOES-10, GMS-5, and MeteoSat-6&7 (Janowiak et al., 2001), while PMW rainfall is calculated from the information provided by TRMM, NOAA-15, -16, -17, DMSP F-13, F-14, and F-15 satellites (Ferraro and Marks, 1995; Kummerow et al., 1998) is used to train the mapping parameters of PERSIANN.

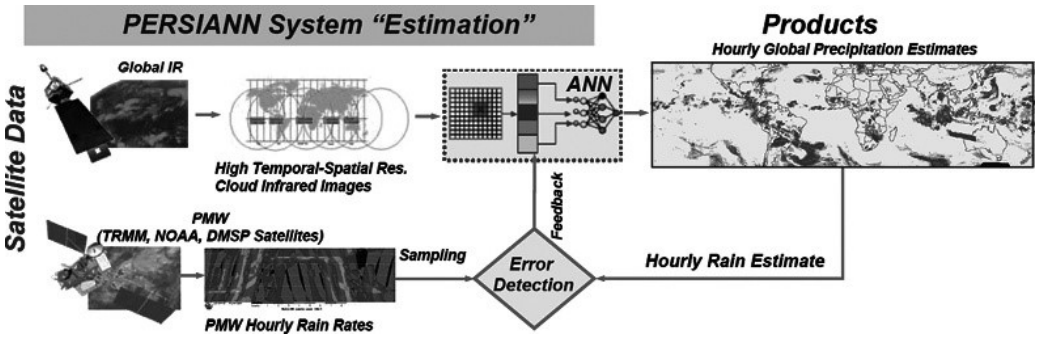

Fig. 1 Rainfall estimation from PERSIANN system using GEO and LEO satellite information (See also Plate 1 in the Colour Plate Section)

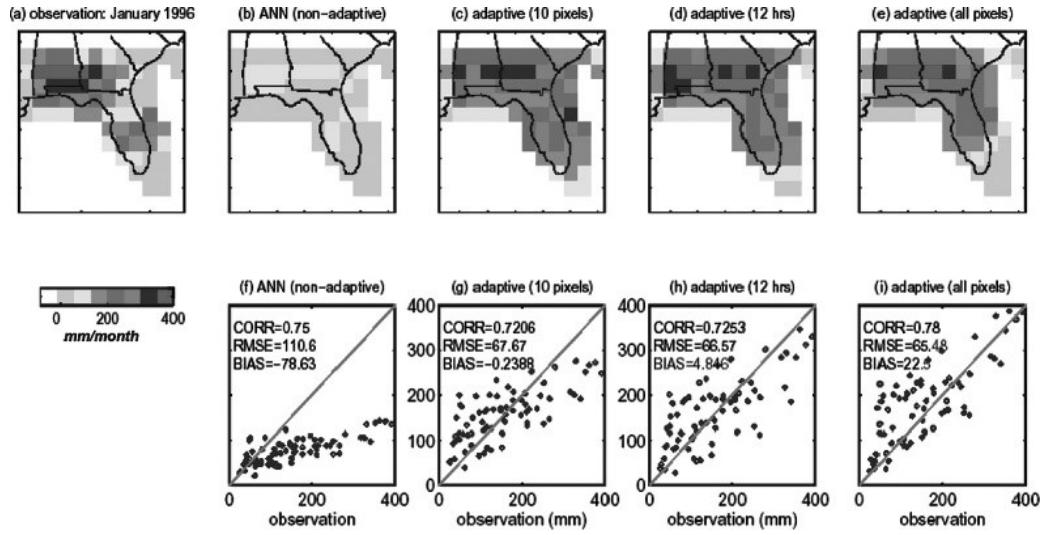

Fig. 2 The adaptive capability of PERSIANN model using limited ground radar rainfall observation over Florida peninsula (See also Plate 2 in the Colour Plate Section)

The simulation of PERSIANN adaptive learning capability using limited rainfall observation from ground radar over Florida peninsula is discussed in Fig. 2. As shown in Fig. 2a, the monthly reference rainfall estimate is provided by the ground-based radar; Fig. 2b shows the monthly PERSIANN estimate of non-adaptive parameter model estimation. As for Fig. 2c, we assumed that hourly ground-based rainfall data are available at only 10 (randomly selected) pixels ($0.25^\circ \times 0.25^\circ$) to simulate the availability of rain gauge data; the scatterplot of radar observation and 10-pixel adjusted PERSIANN estimate is listed in Fig. 2g. In Fig. 2d, we assumed that hourly ground-based rainfall data are available at 12-hour interval to simulate the instantaneous twice-daily rainfall rate estimates of LEO satellites; the scatterplot of radar observation and 12-hour adjusted PERSIANN estimate is listed in Fig. 2h. Finally, the PERSIANN estimate based on all available (every-hour) ground-based radar rainfall samples for adaptive parameter estimation is listed in Fig. 2e; the scatterplot of radar observation and full radar rainfall adjusted PERSIANN estimate is listed in Fig. 2i. Comparison of the three training strategies reveals that the performance improved from the additional information of the training PERSIANN model. In addition, it shows that, compared with the adjusted estimates using partial available data (Fig. 2c,d), the improvement from using all available data (Fig. 2e) is only marginal. Therefore, there is no need to include a large amount of training data.

Demonstration of PERSIANN's capability of using limited TRMM TMI data to display the diurnal pattern of the monsoon season rainfall (June, July, and August 2002) is listed in Fig. 3. The solid-black line calculated is from the NexRAD radar rainfall, while the gray and the dash lines are diurnal rainfall pattern estimated from the adjustment of model parameters with and without using TRMM (2A-12) rainfall data. It shows that the TRMM 2A-12 rainfall adjusted PERSIANN rainfall (gray line) is effective in correcting the underestimated diurnal rainfall pattern (dash-line) toward the referenced radar rainfall pattern (solid-black line).

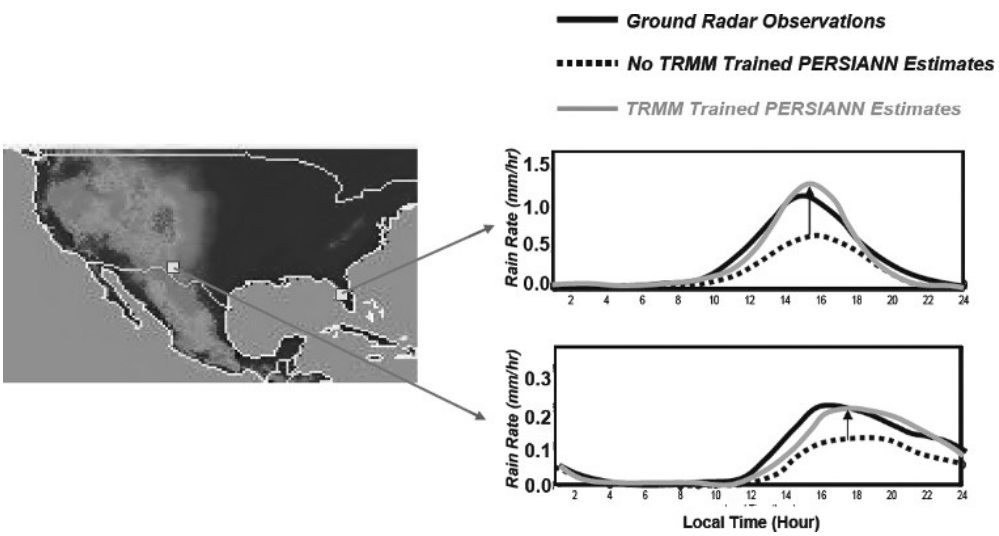

Fig. 3 Diurnal distribution of monsoon rainfall (Summer, 2002) calculated from ground radar observation and PERSIANN estimates with and without TRMM 2A12 rainfall adjustment (See also Plate 3 in the Colour Plate Section)

3 PERSIANN Cloud Classification System (CCS)

The follow on development of the PERSIANN system is to extend the classification features of the GEO IR image from local texture-based to the cloud patch-based features and to improve the resolution of the retrieved product from lower-resolution of $0.25^\circ \times 0.25^\circ$ lat-lon scale to finer resolution of $0.04^\circ \times 0.04^\circ$. The designed patch-based algorithm is named as PERSIANN Cloud-patch Classification System (PERSIANN-CCS). The PERSIANN-CCS patch-based cloud classification and rainfall estimation system is described in Fig. 4. The PERSIANN-CCS consists of four major steps: (1) IR cloud image segmentation, (2) feature extraction from IR cloud patches, (3) patch feature classification, and (4) rainfall estimation. These image processing and computation steps are briefly discussed below. Description of the PERSIANN-CCS can be found from Hong et al. (2004) and Hsu et al., 2007. Those four steps are brief listed below:

(1) Cloud image segmentation: Cloud segmentation is operated through a process that may eventually divide the image into separable patches. This is operated through a watershed-based segmentation approach (Vincent and Soille, 1991). The algorithm starts with finding the local minima temperature of the IR cloud map, followed by raising the IR temperature gradually and connecting the neighborhood pixels attracted to a same local minimum pixel until all the local minimum basins are separated into distinct patches.
(2) Feature extraction: The selected patch features are separated into three categories-coldness, geometry, and texture. From these categories we extract representative features such as the cloud height (coldest temperature), cloud size and shape, surface textures, and surface gradients in our study. In addition,

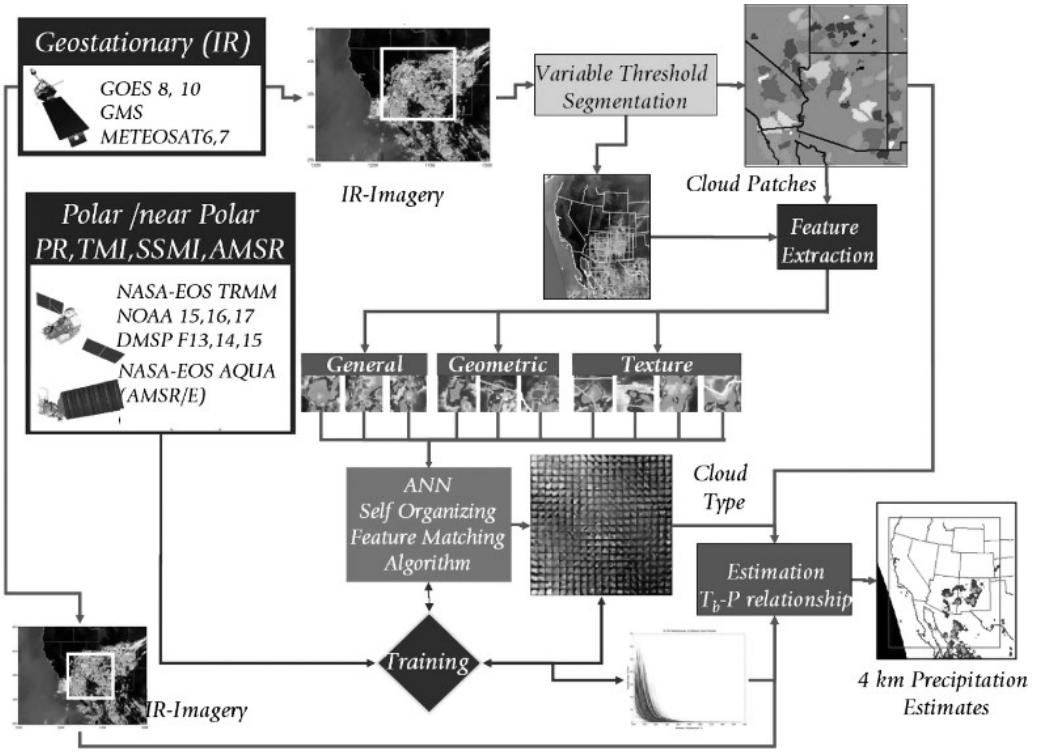

Fig. 4 The data information extraction, classification, and rainfall estimation of PERSIANN-CCS algorithm (See also Plate 4 in the Colour Plate Section)

all the relevant features are extracted from three temperature threshold levels (220K, 235K, and 253K).

(3) Feature classification: Clustering is proceeded based on the similarities of patches measured in their feature spaces. An unsupervised clustering method, Self-Organizing Feature Map (SOFM), is used to classify patch features into a number of cloud patch categories (Kohonen, 1995; Hsu et al., 1999). After training, cloud patches with similar input features are assigned to a same category. An array of 20×20 (i.e. 400) groups was assigned to the classification category. Cloud patches with similar features are grouped together in the same category or assigned to the neighborhood categories.

(4) Specify patch rainfall distribution: The final stage is to specify rainfall distribution to the classified cloud patch categories. At this stage, a large amount of GEO satellite IR image and surface rainfall data is needed. We used one year of radar (over the continental US) and PMW rainfall estimates of LEO satellites (Ferraro and Marks, 1995; Kummerow et al., 1998) to build the rainfall distributions of the classified patch group. The Probability Matching Method (PMM) (Atlas et al., 1990; Rosenfeld et al., 1994) was used to match the relationship between the GEO IR temperature and the hourly rainfall rate in each classified IR patch group, with the assumption that the higher rainfall rate is associated with the lower IR temperature. Finally the $T_b - R$ relationship is fitted by an exponential function of five parameters, where parameters were found from the SCEUA optimization algorithm (Duan et al., 1992).

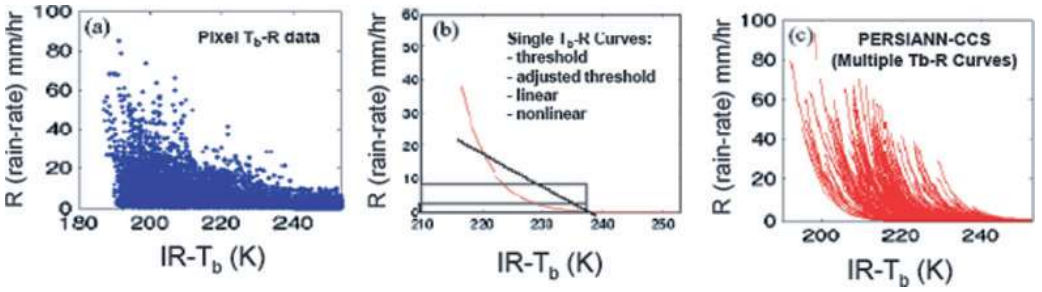

Fig. 5 (a) scatterplot of T_b-R relationship, (b) fitting T_b-R from one-single function, and (c) fitting T_b-R using multiple fitting functions (PERSIANN-CCS)

Figure 5 shows the fitting of the IR brightness temperature (Tb) to the rainfall rate from one-single function and multiple function (PERSIANN-CCS) approaches. The scatterplot of the GEO IR image and radar rainfall (Fig. 5a) shows that the Tb-R relationship is quite wide spread, which cannot be well fitted by a single polynomial curve (see Fig. 5b). Instead of fitting through one single fitting function, approaches were developed to use limited PMW rainfall to correct the Tb-R relationship. Although the results show improvement over those unadjusted estimates, the effectiveness of the algorithms, however, largely relied on the blending procedures to modify the mapping function spatially and temporally.

PERSIANN-CCS, on the other hand, creates a large amount of fitting curve to generate rainfall rates from IR image (see Fig. 5c). With distinguishable features based on IR cloud coldness, size, and textures, each classified cloud patch is assigned a specific Tb-R curve. In the case study, 400 classifications were assigned and therefore multiple Tb-R curves were used to the fitting of the scatter points in Fig. 5a. Compared to other fittings using one-single function, PERSIANN-CCS gives great potential to provide improved estimates.

4 Merging Precipitation Observations from Multiple Sources

Precipitation measurements are available from many sources, including satellites, radar, and gauges. These measurements differ significantly from each other, in terms of scale, resolution, and information contents of their samples. GEO IR and VIS sensors sample cloud top temperature and albedo every 30-minutes, providing information that is indirectly related to surface rainfall rates. PMW sensors carried by LEO satellites sense the water content of rain clouds more directly, but sample the same location only a few (1–2) times per day. In contrast, rain gauges and radar provide much more direct measurements of surface rainfall. However, while rain gauges and radar can provide relatively continuous measurements with high temporal frequency, gauges are sparsely located and provide only point-scale measurements and radar coverage is limited by topography. Because each measurement technology has its own strengths and weaknesses, it is important to develop integrated (merging) approaches that will make the best use of all available information.

Techniques for data smoothing and/or assimilation to combine two or more measurements types, such as objective analysis, Kriging and multi-resolution interpolation, have been suggested (Adler et al., 2000; Huffman et al., 1997; Kumar, 1999; Gorenburg et al., 2001; Gourley et al., 2002; Grimes et al., 1999; Seo and Breidenbach, 2002; Smith and Krajewski, 1991; Xie and Arkin, 1997). Those different techniques vary in their data sources, product scale and coverage, methods for merging (e.g., mean vs. local bias, statistical based method of local bias removal, and recursive scale estimation), and their use of information about uncertainty.

Merging of PERSIANN and other sources of information is also under development. The merging procedure includes either grid-based or watershed based data merging. Our goal, however, is to improve the quality as well as to identify the uncertainty of estimates suitable for hydrologic applications.

4.1 Grid-Based of Data Merging

The uncertainty in satellite precipitation estimates can be highly variable due to many factors such as retrieval technique, weather/climate regime, rainfall type (convective/stratiform), and so on. Usually, bias in satellite precipitation products, such as PERSIANN estimates, can be removed when a given a reference dataset of precipitation is available. After bias is adjusted, the error variance (or random error) of bias corrected estimates can be identified.

4.1.1 Bias Adjustment

For the adjustment of PERSIANN rainfall bias, the Global Precipitation Climatic Centre (GPCC, Rudolf et al., 1994) monthly gauge rainfall product at $1^\circ \times 1^\circ$, monthly resolution is used as a reference data. PERSIANN rainfall product is available at hourly, $0.25^\circ \times 0.25^\circ$ scale. Our assumption is that, with high gauge count, the monthly scale gauge GPCC observed rainfall is more reliable. Therefore, to remove the bias of PERSIANN rainfall, the satellite-based rainfall is accumulated to monthly, $1^\circ \times 1^\circ$, monthly scale. The bias of satellite-based rainfall at the monthly scale is calculated and then downscaled at the monthly $1^\circ \times 1^\circ$ bias spatially and temporally to the basic product level of $0.25^\circ \times 0.25^\circ$ hourly scale. The adjusted satellite rainfall at the monthly scale on the pixel x is calculated below (Kalnay, 2003):

$$Rs_x^a = Rs_x^b + \sum_{i \in \Omega_c} w_i \left[Rg_i - Rs_i^b \right]$$

where Rs_x^b is the before adjusted satellite-based rainfall at calculation pixel x; Rs_x^a is the after adjusted satellite-based rainfall at calculation pixel x; Rg_i is the CPCC monthly rainfall at pixel i; and Ω_x defined a neighborhood region centered at the pixel x; and w_i is a normalized weighting factor being a function of gauge number counts of pixel i, as well as the distance from pixel i to the estimation pixel x, i.e.: $w_i = f(n_i, d_{i \to x})$. The adjusting factor is set to a function of distances and gauge counts:

$$w_i = w_i' \Big/ \sum_{j \in \Omega_x} w_j'$$

where $w_i' = w_{di} \times w_{ni}$,

$$w_{di} = \left(D^2 - d_i^2\right) / \left(D^2 + d_i^2\right), \text{ and}$$
$$w_{ni} = (2 / (1 + \exp(-\alpha\, n_i)) - 1 \text{ and } w_{ni} = 0.1 \text{ if } w_{ni} \leq 0.1$$

The w_{ni} is the distance weighting factor from the pixel i to the pixel x and w_{di} is the gauge density weighting factor at pixel i, respectively; D is the maximum effective distance from center pixel x; d_i is the distance between center calculation pixel x to a pixel i; α is a factor related to the gauge counts in the pixel i; a smaller α has a higher slope with respect to the gauge count.

This adjustment is run through several iterations until a stable adjusted rainfall is obtained. Assuming that the errors of $1^\circ \times 1^\circ$ resolution pixels are positive proportional to the satellite-based rainfall at fine spatial and temporal scale, the calculated monthly adjustment error at x of $1^\circ \times 1^\circ$ grid is then downscaled to the fine resolution grids of hourly and $0.25^\circ \times 0.25^\circ$.

Figure 6 shows an example of using $1^\circ \times 1^\circ$ GPCC monthly rainfall for the spatial and temporal adjustment of PERSIANN rainfall bias and then the monthly bias is downscaled to the PERSIANN rainfall at $0.25^\circ \times 0.25^\circ$ six-hour accumulated resolution. Compared with the NCEP Stage IV radar rainfall, the consistent bias and the RMSEs error in PERSIANN estimates are reduced substantially during July 2001. In our follow on activity, the same bias adjustment procedure is applied to remove the bias correction of PERSIANN-CCS rainfall at 0.04×0.04 hourly scale using daily and $0.25^\circ \times 0.25^\circ$ CPC precipitation analysis.

4.1.2 Variance Quantification

When the product bias is corrected, we could further calculate the random error of the product based on a reliable reference source, such as gauge or radar measurements. In the calculation of the error variance of PERSIANN estimates, we use NCEP radar stage IV radar rainfall as the reference data source. This error variance here is a relative error statistics related to a selected reference, such as the NCEP stage IV radar rainfall in our case. The reliable error variance of PERSIANN estimates can be estimated further using an error variance separation approach when the error variance of NECP radar rainfall is identified (Anagnostou et al., 1999; Ciach and Krajewski, 1999; Gebremichael et al., 2003). It is also assumed that the error variance V_E of the PERSIANN product is a function of the product at its temporal resolution T, spatial resolution L, as well as the rainfall rate r (Hong et al., 2006; Steiner et al., 2003). The scaling property of PERSIANN rainfall random error, σ_E, is represented as:

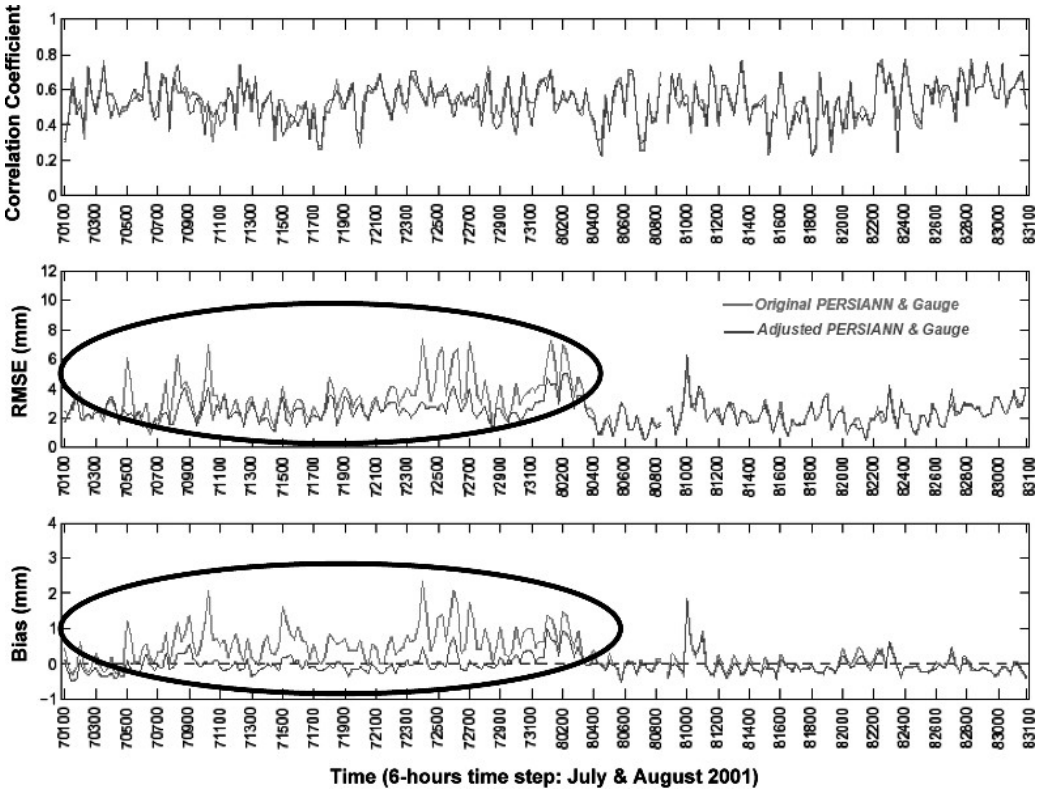

Fig. 6 Evaluation of original (*blue-line*) and GPCC month gauge data corrected (*red-line*) PERSIANN six-hour rainfall using NCEP stage IV radar estimates in U.S. Although the correlation coefficients (**upper panel**) are similar for both original and bias correction PERSIANN rainfalls; the biases and RMSEs are significant improved in July 2001 for the bias corrected PERSIANN rainfall (See also Plate 5 in the Colour Plate Section)

$$\sigma_E = a \cdot \left(\frac{1}{L}\right)^b \cdot \left(\frac{1}{T}\right)^c (r)^d$$

where a, b, c, and d are the parameters to be determined by calibration and the units for L, T, and r are degrees of lat.-lon., hour, and mm hr^{-1}, respectively. In our experiment, parameters of the error model were calculated from the summer period of 2003 and 2004 using both PERSIANN and NCEP stage IV radar rainfall. Application of the PERSIANN product error in the evaluation of hydrologic model responses will be discussed later.

4.2 Basin Scale Merging of Gauge and Satellite Rainfall

Another merging approach is to consider that the rainfall measurement from gauge and satellites are subject to bias and random error. The basin scale merged rainfall is parameterized based on the gauge and satellite observed rainfall data, and extendable to other sources, such as the radar rainfall below:

$$r_m(t) = w_s(1 - b_s)r_s(t) + w_g(1 - b_g)r_g(t)$$

where, $r_m(t)$ is the merged averaged rain rate, $r_s(t)$ is the satellite-based (PERSIANN) rain rate, and $r_g(t)$ is the observed gauged rain rate; w_s and w_g are the merging weights for the satellite rain rate $r_s(t)$ and the simultaneous gauge rain rate $r_g(t)$, respectively; b_s and b_g are the bias parameters of r_s and r_g. It is understandable that in the merging equation, the b_s and b_g is the bias of r_s and r_g (assuming that the rainfall bias is positive proportional to rain rate), and w_s and w_g are the weighting factor of bias-removed r_s and r_g.

In the catchment scale hydrologic simulation, by applying the merged rainfall data $r_m(t)$ to the hydrological forecast system, the consequent streamflow $q(t)$ is generated. An optimal set of those parameters $\vec{\theta} = [w_s, w_g, b_s, b_g]$ is obtained by maximizing the likelihood function of modeled streamflow, q(t), and its observations, $q_o(t)$. The distribution of $\vec{\theta}$ can be estimated from the Monte Carlo Simulation techniques (Doucet et al., 2000; Gelman et al., 1995; Robert and Casella, 2004). Let's say the precipitation merging parameters are defined as $\vec{\theta}$. Given the streamflow observation time series: $D = \{r_s(t), r_g(t), q_o(t)\}$, t=1...T, the most plausible parameters $\vec{\theta}$ can be calculated from the Bayes' rule below:

$$P(\vec{\theta}|D) = P(D|\vec{\theta})P(\vec{\theta})/P(D)$$

where $P(D) = \sum P(D|\vec{\theta})P(\vec{\theta})$ is the total probability, while $P(\vec{\theta})$ is the a priori probability of the parameters, $\vec{\theta}$. The factor $P(D|\vec{\theta})$ is the likelihood function of the parameters provided by the data D, and $P(\vec{\theta}|D)$ is the posterior distribution of parameters given by a set of data D. The posterior distribution presents the relevant information in the data and provides a summary of post-data uncertainty.

From the Monte Carlo simulation through a calibrated hydrologic model, the distribution of parameters ($\vec{\theta}$ and the merged precipitation can be calculated. Through the simulation of a hydrologic model, the uncertainty of merged rainfall, hydrologic state variables, as well as the streamflow forecasts can be estimated.

A case study of combining gauge and satellite-based rainfall using basin-scale merging method was tested. The size of the test watershed (Leaf-River Basin) was around 1949 km^2. The National Weather Service Soil Moisture Accounting SACramental model (SAC-SMA) was used to generate streamflow from the merged rainfall; the SAC-SMA model parameters were set to the default parameters, which were calibrated from long years of historical data.

The upper panels of Fig. 7 show the rainfall time series from the basin averaged gauge rainfall, PERSIANN rainfall, and merged gauge-PERSIANN rainfall, respectively. The lower panel shows the streamflow responses with input rainfall time series from the gauge, PERSIANN, and merged rainfall. The plot with the square symbol is the observed streamflow. The performance indexes of the hydrologic streamflow forecasting given the precipitation forcing from the gauge, PERSIANN, merged rainfall were calculated. These statistics include root mean square error (RMSE), correlation coefficient (CC), and bias (BIAS) listed below:

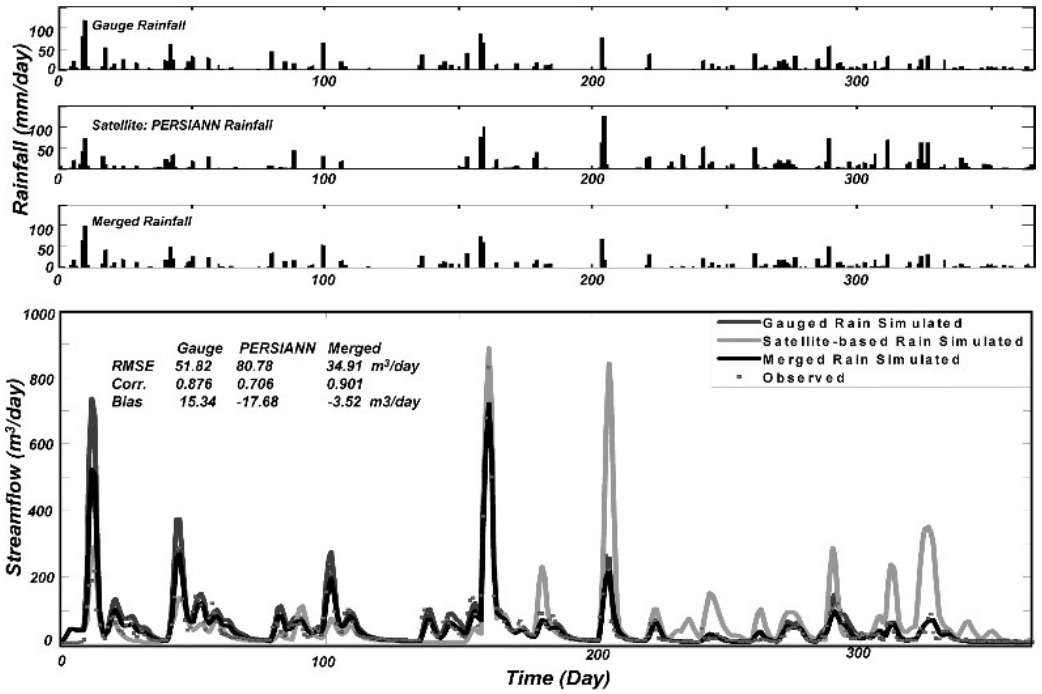

Fig. 7 The top three panels show the gauge, PERSIANN, and merged rainfall, respectively; The bottom panel shows the streamflow responses from gauge rainfall (*blue-line*), PERSIANN rainfall (*green-line*), and merged rainfall (*black-line*). Observed Streamflow is shown in *red dots* (See also Plate 6 in the Colour Plate Section)

$$\text{RMSE}\{\text{Gauge, PERSIANN, Merged rainfall}\} = \{51.82, 80.78, 34.91\} \text{ cmsd;}$$
$$\text{CORR}\{\text{Gauge, PERSIANN, Merged rainfall}\} = \{0.876, 0.706, 0.901\}$$
$$\text{BIAS}\{\text{Gauge, PERSIANN, Merged rainfall}\} = \{15.34, -17.68, -3.52\} \text{ cmsd.}$$

From the performance statistics, in terms of RMSE, CORR, and BIAS, input forcing that uses the merged rainfall source outperforms those using either gauge or satellite-based rainfall.

The 95% conference bound of merged rainfall is listed in Fig. 8. With the uncertainty of precipitation forcing provided, the uncertainty of streamflow forecasts from the forcing uncertainty can be further derived.

5 Evaluation and Hydrologic Application of PERSIANN Rainfall

The operational PERSIANN precipitation data has continued to provide the IPWG precipitation product evaluation on a regular basis. Figure 9 shows the visual display of PERSIANN precipitation estimates, and the relevant information is available at: http://hydis8.eng.uci.edu/hydis-unesco/. The product is generated at every 30 minutes at the resolution of $0.25^\circ \times 0.25^\circ$ scales. In addition, the high resolution PERSIANN-CCS estimates are available from: http://hydis8.eng.uci.edu/CCS/.

Due to the lack of independent observations at sub-daily scale over global coverage, only limited validation sources were used for the evaluation of PERSIANN

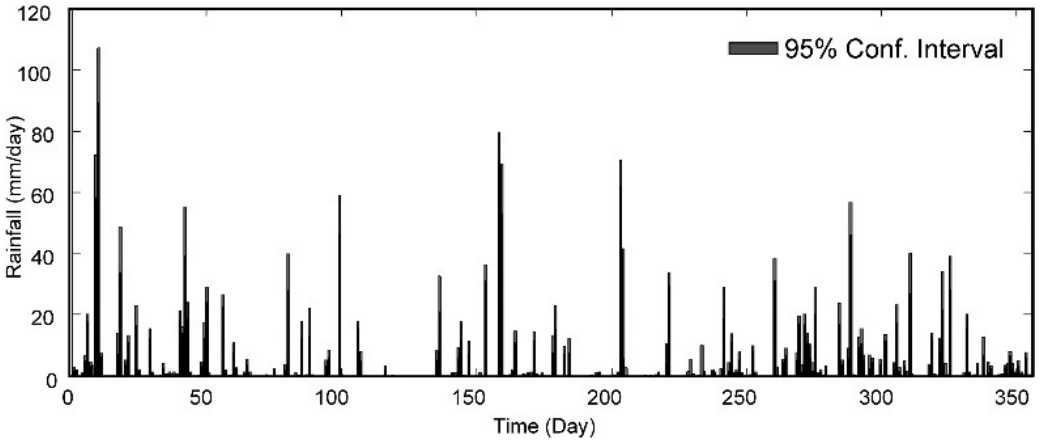

Fig. 8 Merged rainfall time series and 95% confidence interval (*red-bar*) of merged rainfall (See also Plate 7 in the Colour Plate Section)

data. PERSIANN validation activities can be found from Hong et al. (2004, 2005); Hsu et al. (1997, 1999); Sorooshian et al. (2000, 2002); Yilmaz et al. (2005).

As displayed in Fig. 10, the monthly PERSIANN rainfall data were evaluated for locations consisting of more than five gauges in the area coverage of $5^\circ \times 5^\circ$ around the low- to mid-latitude of continents around the Pacific Ocean (Sorooshian et al., 2000, for detail). Those selected grid boxes are listed in Fig. 10a. The scatterplots (Fig. 10b–d) show that the fitting is quite good (correlation coefficient $\varrho > 0.77$) and improves for cells having larger numbers of gauges. For grid boxes with more than 10 gauges, the correlation increases to 0.9, while the root mean square error reduces to 59 mm/month, and the bias shows a tendency to overestimate.

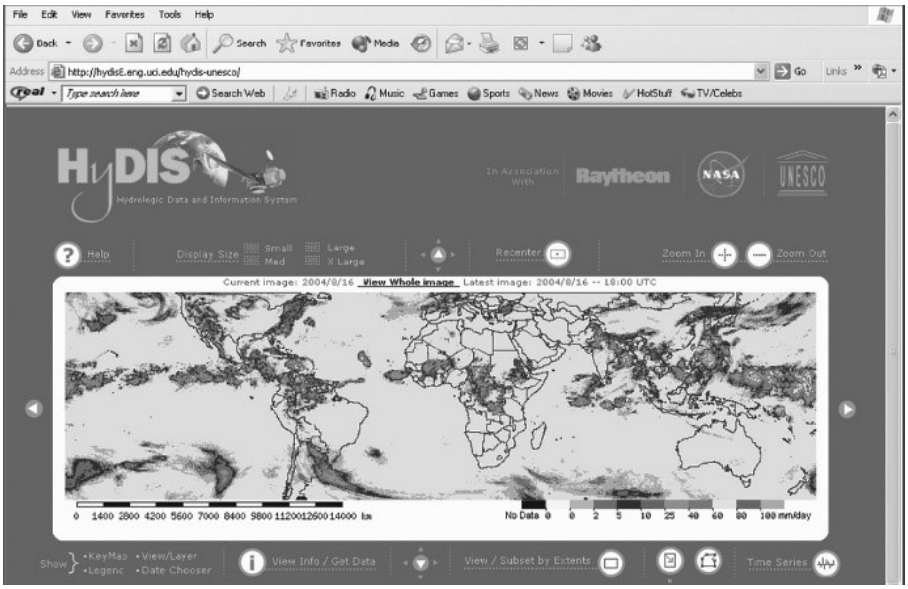

Fig. 9 The visual display of PERSIANN precipitation estimates and relevant information is available through: http://hydis8.eng.uci.edu/hydis-unesco/ (See also Plate 8 in the Colour Plate Section)

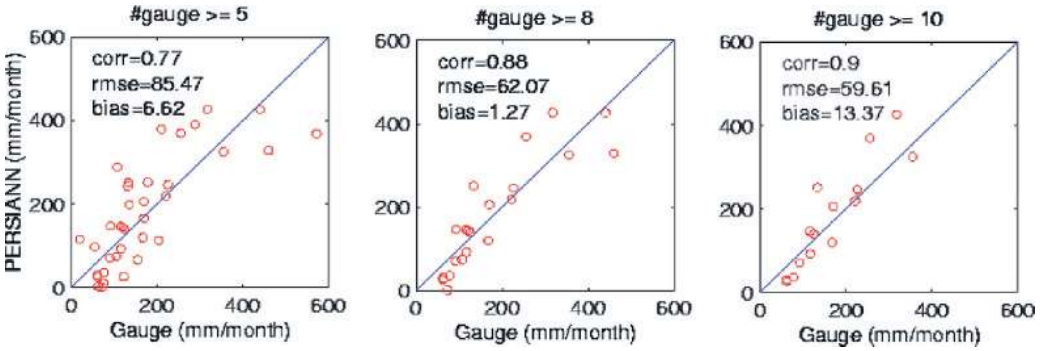

Fig. 10 Monthly rainfall from PERSIANN and GPCC gauge data for gauge count greater than (a) 5 gauges, (b) 8 gauges, and (c) 10 gauges in $5^\circ \times 5^\circ$ grid boxes

For a finer scale of evaluation, around two months (January 7–February 28, 1999) of TRMM field campaign precipitation data observed from TOGA radar near Rondonia Brazil were used. Evaluation was done at daily rainfall at $1^\circ \times 1^\circ$ and the diurnal rainfall pattern in the radar coverage. The result shows in Fig. 11, for the daily rainfall at $1^\circ \times 1^\circ$ grid boxes, the correlation coefficients of PERSIANN and radar rainfall is around 0.68–0.77. For averaged diurnal cycle of rainfall in the testing 2-month period, the peak-hour of diurnal PERSIANN rainfall tends to have approximately 1-hour lag from the radar-based rainfall. The maximum diurnal rainfall of PERSIANN's is similar to the radar estimates, but it tends to be extended for a longer duration from the potential contamination by the cold anvil cirrus clouds (Sorooshian et al., 2000).

Although many several satellite-based rainfall evaluation activities had been conducted in the past years, most of the evaluations focused at climate scales of lower

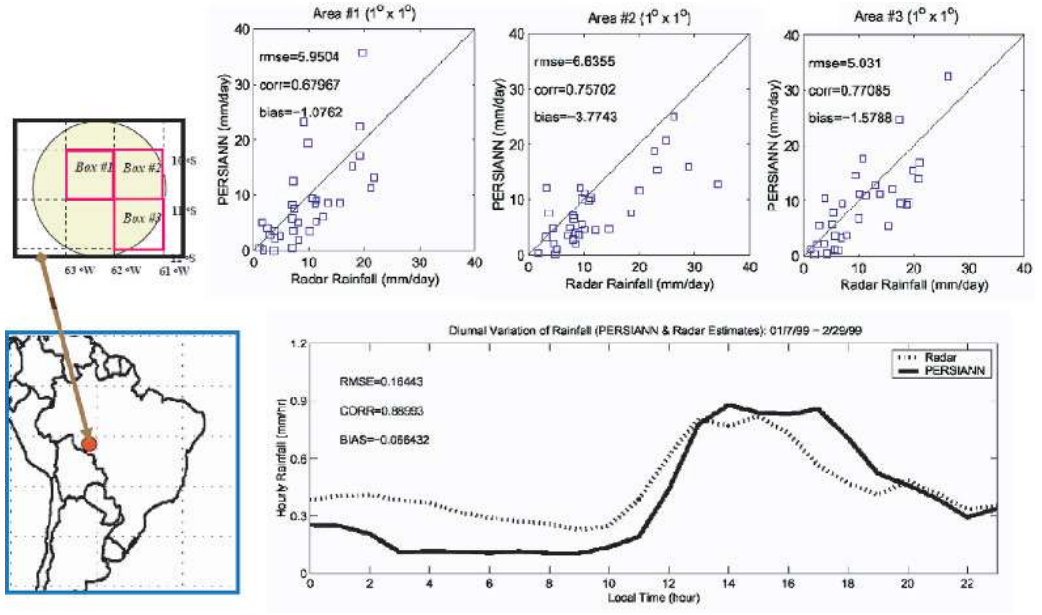

Fig. 11 Evaluation of PERSIANN rainfall based on TRMM field campaign precipitation data observed from TOGA radar near Rondonia, Brazil (January 7–February 28, 1999)

spatial and temporal resolution (Adler et al., 2001; Arkin and Xie, 1994; Ebert et al., 1996). Although some recent developed algorithms using merged IR/VIS and PMW information are considered to be capable of providing finer spatial and temporal resolution precipitation estimates (e.g. Huffman et al., 2002; Joyce et al., 2004; Kuligowski, 2002; Sorooshian et al., 2000; Tapiador, 2004; Turk et al., 2000; Vicente et al., 1998), they have not been systematically evaluated. Recently, the International Precipitation Working Group (IPWG) initiated a satellite-based precipitation evaluation program to cover three regions, including:

(1) United States: (see: http://www.cpc.ncep.noaa.gov/products/janowiak/us_web.shtml),
(2) Australia: (see: http://www.bom.gov.au/bmrc/SatRainVal/sat_val_aus.html), and
(3) Europe (see: http://kermit.bham.ac.uk/∼kidd/ipwg_eu/ipwg_eu.html).

A number of satellite-based precipitation products were evaluated at daily, $0.25^\circ \times 0.25^\circ$ lat-lon scale. The evaluation activities of IPWG are ongoing and further extended to the program of the Pilot Evaluation of High Resolution Precipitation Products (PEHRPP). This program includes a few additional regions for validation from several scales (monthly, daily, and sub-daily) as well as to include evaluation using high quality field observations (Arkin et al., 2005; Turk et al., 2006). The global PERSIANN precipitation estimates are routinely evaluated. The results of the evaluation program provide important information of the model capability to crossover various seasons and climate regions. Figure 12 shows the evaluation of PERSIANN rainfall over Australia, hosted by Bureau of Meteorology Research Centre, Australia (http://www.bom.gov.au/bmrc/SatRainVal/sat_val_aus.html).

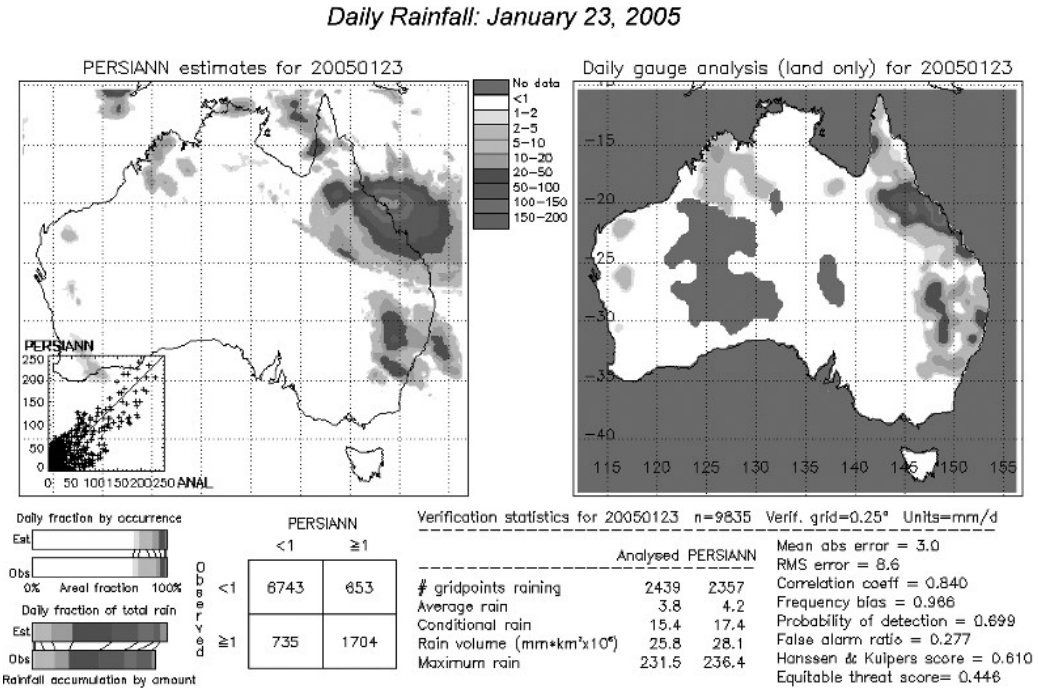

Fig. 12 PERSIANN evaluation over Australia region (See also Plate 9 in the Colour Plate Section)

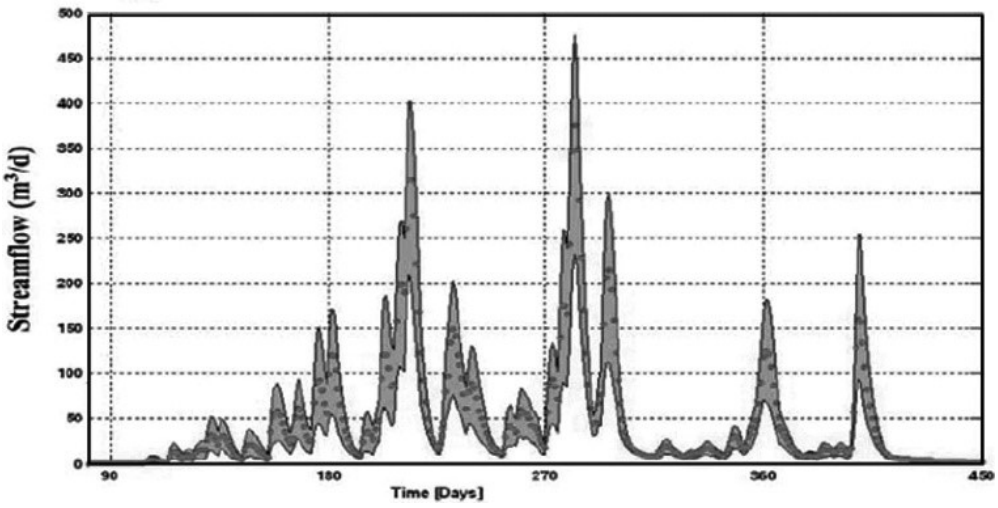

Fig. 13 Uncertainty of hydrologic response with respect to the PERSIANN rainfall uncertainty (See also Plate 10 in the Colour Plate Section)

PERSIANN products have been used in a number of hydrologic applications. These studies have included: comparison of mean areal precipitation with rain gauge and NEXRAD radar estimates; evaluation of MM5 numerical weather forecast model estimates over the Southwest U.S., Mexico, and adjacent oceanic regions (Li et al., 2003a,b); assimilation into a Regional Atmospheric Modeling System (RAMS) model for the Southwest United States to investigate land-surface hydrologic process including soil moisture (Yi, 2002); evaluation the sensitivity of convective parameterization of MM5 model in the simulation of the climate in the North American Monsoon region (Gochis et al., 2002); documentation of the diurnal rainfall pattern of tropical and mid-latitude regions (Sorooshian et al., 2002; Hong et al., 2005); intercomparison of gauge, radar, and satellite-based estimates in hydrologic forecasting (Yilmaz et al., 2005); and the uncertainty analysis of hydrologic responses due to the forcing precipitation uncertainty (Hong et al., 2006; Moradkhani et al., 2006).

Figure 13 shows the hydrologic response with consideration of the input forcing uncertainty (PERSIANN rainfall). The scale dependent error variance of PERSIANN rainfall is calculated based on the catchment size and time scale (daily) of the simulation. The 95% confidence of the steamflow response from the Monte Carlo simulation of PERSIANN precipitation and its error variance property through a conceptual rainfall-runoff model is obtained (Hong et al., 2006). Further consideration of the uncertainty of the input forcing and initial condition of states of hydrologic model was also explored and discussed in Moradkhani et al. (2006).

6 Summary

In this paper, the development of the PERSIANN system and its continuing evolution during the past years was presented. The advantages of the proposed PERSIANN system include: (1) its flexibility to include various types of testing features,

(2) automatic classification process, and (3) effective mapping capability. PERSIANN system is considered as a data merging/fusion algorithm for precipitation retrieval from multiple satellites. The adaptive training feature of PERSIANN also makes it easy to make better use of both the effective sampling capability at every 30 minutes interval from GEO satellites and the better quality PMW sensors but less frequent samples of LEO satellites.

Input features of PERSIANN consist of the statistics of local texture (mean and standard deviation of the brightness temperature of neighborhood pixels) of thermal IR channel of GEO satellites. They were also tested to include the VIS channel and it was shown to be rather effective in the day-time rainfall retrieval. However, for the simplicity of the regular operation, only thermal IR image were used, which enables the algorithm to be directly applied to the full-day and all-weather conditions. The development of PERSIANN extended the input features and classification system from local texture-based to the regional cloud patch-based. This led to the development of the PERSIANN-CCS algorithm. The PERSIANN-CCS algorithm separates the disjointed thermal IR cloud image into disjointed cloud patches and then extracts the patch features and classifies them into several patch categories. Each classified category is assigned a specific rainfall distribution. The PERSIANN-CCS generates estimates at hourly and $0.04^\circ \times 0.04^\circ$ lat-lon scale. Routine operation of PERIANN-CCS is underdevelopment.

Precipitation is a major forcing variable to the land surface hydrologic process. The uncertainty of precipitation estimates has important consequences to the streamflow response of a catchment. With the interest of data quality in mind, our continuing effort has been in quantifying the uncertainty of satellite-based rainfall through available ground observations. This has been conducted through the bias correction of PERSIANN rainfall at lower spatial and temporal scale (e.g. daily and $0.25^\circ \times 0.25^\circ$) and then to downscale the bias to high spatial and temporal resolutions, for example hourly $0.04^\circ \times 0.04^\circ$. In addition, for the catchment scale, a merging method that combines observations from gauge, radar, and satellite-based observed rainfall, is under investigation. This approach is being implemented at the catchment scale and has the potential to provide a better merged precipitation product for basin scale hydrologic simulation.

Acknowledgments The authors wish to acknowledge the support provided by NOAA, NASA and NSF under various grants over the years. Research data is made available from NCDC, NWS, NESDIS and CPC of NOAA, and TRMM program of NASA. The Authors would like to thank the current and past students and colleagues (D. Braithwaite, F. Isak-Boushaki, X. Gao, H.V. Gupta, Y. Hong, B. Imam, J. Li, S. Mahani, H. Moradkhani, G.-H. Park, and K. Yilmaz) who have been involved in the development of the precipitation retrieval algorithms and PERSIANN data applications. Mrs. Diane Hohnbaum's assistance in proofreading the manuscript is very much appreciated.

The authors also wish to express appreciation to the University of L' Aquila and CETEMPS as well as Regione Abruzzo and the National Civil Protection Agency of Italy for their support of the workshop. Many thanks to Dr. Erika Coppola who co-directed the workshop; the support of the local organizing committee of Drs. Marco Verdecchia, Barbara Tomassetti and Guido Visconti is much appreciated.

References

Adler, R.F., J.A. Negri, P.R. Keehn, and I.M. Hakkarinen, 1993: Estimation of monthly rainfall over Japan and surrounding waters from a combined of low-orbit microwave and geosynchronous IR data. *Journal of Applied Meteorology*, **32**, 335–356.

Adler, R.F., G.J. Huffman, D.T. Bolvin, S. Curtis, and E.J. Nelkin, 2000: Tropical rainfall distributions determined using TRMM combined with other satellite and rain gauge information. *Journal of Applied meteorology*, **39**, 2007–2023.

Anagnostou, E.N., W.F. Krajewski, and J.A. Smith, 1999: Uncertainty quantification of mean-areal radar rainfall estimates. *Journal Atmospheric Oceanic Technology*, **16**(2), 206–215.

ASCE Task Committee on Application of Artificial Neural Networks in Hydrology, 2000: Artificial neural network in hydrology. II: Hydrologic applications. *Journal of Hydrologic Engineering*, ASCE **5**(2), 124–137.

Adler, R.F., C. Kidd, G. Petty, M. Morrissey, and H.M. Goodman, 2001: Intercomparison of global precipitation products: the third precipitation intercomparison project (PIP–3). *Bulletin of the American Meteorological Society*, **82**, 1377–1396.

Arkin, P.A. and P. Xie, 1994: The global precipitation climatology project: first algorithm intercomparison project. *Bulletin of the American Meteorological Society*, **75**, 401–419.

Arkin, P.A., J. Turk, and E. Ebert, 2005: Pilot Evaluation of High Resolution Precipitation Products (PEHRPP): a contribution to GPM planning. 5th Global Precipitation Mission (GPM) Planning Workshop, Tokyo, Japan, 7–9 November 2005.

Atlas, D., D. Rosenfeld, and D. Short, 1990: The estimation of convective rainfall by area integrals. 1. The theoretical and empirical basis. *Journal Geophys Research*, **95**(D3), 2153–2160.

Ba, M.B. and A. Gruber, 2001: GOES multispectral rainfall algorithm (GMSRA), *Journal of Applied Meteorology*, **40**, 1500–1514.

Bellerby, T., M. Todd, D. Kniveton, and C. Kidd, 2000: Rainfall estimation from a combination of TRMM precipitation radar and GOES multispectral satellite imagery through the use of an artificial neural network. *Journal of Applied Meteorology*, **39**, 2115–2128.

Ciach, G.J. and W.F. Krajewski, 1999: On the estimation of radar rainfall error variance. *Advanced Water Resources*, **22**, 585–595.

Committee on the Future of the Tropical Rainfall Measuring Mission, National Research Council, 2004: Assessment of the Benefits of Extending the Tropical Rainfall Measurement Mission: A Perspective from the Research and Operations Communities, Interim Report, National research Council of the National Academies, The National Academies Press, Washington, D.C.

Coppola, E., D.I.F. Grimes, M. Verdecchia and G. Visconti, 2006: Validation of improved TAMANN neural network for operational satellite-derived rainfall estimation in Africa, *Journal of Applied Meteorology*, **45**(11), 1557–1572.

Doucet, A., S. Godsill, and C. Aadrieu, 2000: On sequential Monte Carlo sampling methods for Bayesian filtering. *Statistics and Computing*, **10**, 197–208.

Duan, Q., S. Sorooshian, and V.K. Gupta, 1992: Effective and efficient global optimization for conceptual rainfall-runoff model. *Water Resources Research*, **28**(4), 1015–1031.

Ebert, E.E., M.J. Manton, P.A. Arkin, R.J. Allam, G.E. Holpin, and A.J. Gruber, 1996: Results from the GPCP algorithm intercomparison programme. *Bulletin of the American Meteorological Society.* **77**, 2875–2887.

Ebert, E.E. and M.J. Manton, 1998: Performance of satellite rainfall estimation algorithms during TOGA COARE, *Journal of Atmospheric Science*, **55**, 1537–1557.

Ebert, E.E, J.E. Janowiak, and C. Kidd, 2006: Comparison of near real time precipitation estimates from satellite observations and numerical models. *Bulletin of the American Meteorological Society*. (In review).

Ebert, E.E., J.E. Janowiak, and C. Kidd, 2007: Comparison of near real time precipitation estimates from satellite observations and numerical models. *Bulletin of the American Meteorological Society*. **88**(1), 47–64.

Ferraro, R.R. and G.F. Marks, 1995: The development of SSM/I rain-rate retrieval algorithms using ground-based radar measurements. *Journal of Atmospheric Oceanic Technology*, **12**, 755–770.

Gebremichael, M., W.F. Krajewski, M. Morrissey, D. Langerud, G.J. Huffman, and R. Adler, 2003: Error uncertainty analysis of GPCP monthly rainfall products: a data-based simulation study, *Journal of Applied Meteorology*, **42**, 1837–1848.

Gelman, A., J.B. Carlin, H.S. Stern, and D.B. Rubin, 1995: *Bayesian Data Analysis*. London: Chapman and Hall. First edition.

Gochis, D.J., W.J. Shuttleworth, and Z.-L. Yang, 2002: Sensitivity of the modeled North American Monsoon regional climate to convective parameterization. *Monthly Weather Review*, **130**, 1282–1298.

Gorenburg, I.P., D. McLaughlin, and D. Entekhabi, 2001: Scale-recursive assimilation of precipitation data. *Advances in Water Resources*, **24**, 941–953.

Gourley, J.J., R.A. Maddox, K.W. Howard, and D.W. Burgess, 2002: An exploratory multisensor technique for quantitative estimation of stratiform rainfall. *Journal of Hydrometeorology*, **3**(2), 166–180.

Govindaraju, R.S. and A.R. Rao, 2000: *Artificial Neural Networks in Hydrology*. Dordrecht: Kluwer Academic Publishers, 329pp.

Grimes, D.I.F., E. Pardo-Iguzquiza, and R. Bonifacio, 1999: Optimal areal rainfall estimation using raingauges and satellite data. *Journal of Hydrology*, **222**, 93–108.

Grimes, D.I.F., E. Coppola, M. Verdecchia, and G. Visconti, 2003: A neural network approach to real-time rainfall estimation for Africa using satellite data. *Journal of Hydrometeorology*, **4**(6), 1119–1133.

Hong, Y., K. Hsu, X. Gao, and S. Sorooshian, 2004: Precipitation estimation from remotely sensed information using an artificial neural network—Cloud classification system. *Journal of Applied Meteorology*, **43**, 1834–1852.

Hong, Y., K. Hsu, S. Sorooshian, and X. Gao, 2005: Enhanced signal of diurnal variability of rainfall retrieval from TRMM-adjusted PERSIANN algorithm. *Journal of Geophysical Research*, **110**, D06102.

Hong, Y., K. Hsu, H. Moradkhani, and S. Sorooshian, 2006: Uncertainty quantification of satellite precipitation estimation and Monte Carlo assessment of the error propagation into hydrologic response. *Water Resources Research*, **42**, W08421.

Hou, A.Y., 2006: The Global Precipitation Measurement (GPM) Mission: An Overview. EGU General Assembly 2006, Vienna, Austria, 2–7 April.

Hsu, K., X. Gao, S. Sorooshian, and H.V. Gupta, 1997: Precipitation estimation from remotely sensed information using artificial neural networks. *Journal of Applied Meteorology*, **36**, 1176–1190.

Hsu, K., H.V. Gupta, X. Gao, and S. Sorooshian, 1999: A neural network for estimating physical variables from multi-channel remotely sensed imagery: application to rainfall estimation. *Water Resources Research*, **35**, 1605–1618.

Hsu, K., Y. Hong, and S. Sorooshian, 2007: Rainfall estimation using a cloud patch classification map, In Measurement of Precipitation from Space: EURAINSAT and Future, Edited by V. Levizzani, P. Bauer, and F.J. Turk. Springer, Dordrecht, The Netherlands.

Huffman, G.J., R.F. Adler, P.A. Arkin, A. Chang, R. Ferraro, A. Gruber, J.E. Janowiak, A. McNab, B. Rudolf, and U. Schneider, 1997: The Global Precipitation Climatology Project (GPCP) combined precipitation dataset. *Bulletin of the American Meteorological Society*, **78**, 5–20.

Huffman, G.J., R.F. Adler, M. Morrissey, D.T. Bolvin, S. Curtis, R. Joyce, B. McGavock, and J. Susskind, 2001: Global precipitation at one-degree daily resolution from multi-satellite observations. *Journal of Hydrometeorology*, **2**, 36–50.

Huffman, G.J., R.F. Adler, E.F. Stocker, D.T. Bolvin, and E.J. Nelkin, 2002: A TRMM-based system for real-time quasi-global merged precipitation estimates. TRMM International Science Conference, Honolulu, 22–26 July 2002.

Kumar, P., 1999: A multiple scale state-space model for characterizing subgrid scale variability of near-surface soil moisture. *IEEE Transactions on Geoscience and Remote Sensing*, **37**(1), 182–197.

Janowiak, J.E., R.J. Joyce, and Y. Yarosh, 2001: A real-time global half-hourly pixel-resolution infrared dataset and its applications. *Bulletin of the American Meteorological Society*, **82**, 205–217.

Joyce, R.J., J.E. Janowiak, P.A. Arkin, and P. Xie, 2004: CMORPH: a method that produces global precipitation estimates from passive microwave and infrared data at high spatial and temporal resolution. *Journal of Hydrometeorology*, **5**, 487–503.

Kalnay, E., 2003: Atmospheric Modeling, *Data Assimilation and Predictability*, Cambridge University Press, Cambridge, UK.

Kohonen, T., 1995: *Self-Organizing Map*, Springer-Verlag, New York.

Krasnopolsky, V.M. and H. Schiller, 2003: Some neural network applications in environmental sciences. Part I: Forward and inverse problems in geophysical remote measurements. *Neural Networks*, **16**, 321–334.

Krasnopolsky, V.M. and F. Chevallier, 2003: Some neural network applications in environmental sciences. Part II: Advancing computational efficiency of environmental numerical models. *Neural Networks*, **16**, 335–348.

Kuligowski, R.J., 2002: A self-calibrating real-time GOES rainfall algorithm for short-term rainfall estimates. *Journal of Hydrometeorology*, **3**, 112–130.

Kummerow, C., W. Barnes, T. Kozu, J. Shiue, and J. Simpson, 1998: The tropical rainfall measurement mission (TRMM) sensor package. *Journal of Atmospheric Oceanic Technology*, **15**, 809–816.

Kummerow, C., J. Simpson, O. Thiele, W. Barnes, A.T.C. Cgang, E. Stocker, R.F. Adler, A. Hou, R. Kakar, F. Wentz, P. Ashcroft, T. Kuzu, Y. Hong, K. Okamoto, T. Iguchi, H. Kuroiwa, E. Im, Z. Haddad, G. Huffman, B. Ferrier, W.S. Olson, E. Ziper, E.A. Smith, T.T. Wilheit, G. North, T. Krishnamurti, and K. Nakamura, 2000: The status of the tropical rainfall measuring mission (TRMM) after two years on orbit. *Journal of Applied meteorology*, **39**, 1965–1982.

Levizzani, V., P. Bauer, and F.J. Turk, 2007: Measurement of Precipitation from Space: EURAINSAT and Future, Springer, Dordrecht, The Netherlands.

Li, J., X. Gao, R.A. Maddox, S. Sorooshian, and K. Hsu, 2003a: Summer weather simulation for the semi-arid lower Colorado river basin: case tests. *Monthly Weather Review*, **131**(3), 521–541.

Li, J., X. Gao, R.A. Maddox, S. Sorooshian, and K. Hsu, 2003b: A numerical investigation of the storm structure and evolution in the 1999 Las Vegas flooding. *Monthly Weather Review*, **131**(9), 2038–2059.

Maier, H.R. and G.C. Dandy, 2000: Neural networks for prediction and forecasting of water resources variables: a review of modeling issues and applications. *Environmental Modeling and Software*, **15**, 101–124.

Miller, S.W., P.A. Arkin, and R. Joyce, 2001: A combined microwave/infrared rain rate algorithm. *International Journal of Remote Sensing*, **22**, 3285–3307.

Moradkhani, H., K. Hsu, Y. Hong, and S. Sorooshian, 2006: Investigating the impact of remotely sensed precipitation and hydrologic model uncertainties on the ensemble streamflow forecasting. *Geophysical Research Letters*, **33**(12), L12107, 10.1029/2006GL026855.

Marzano, F.S., M. Palmacci, D. Cimino, G. Giuliano, and F.J. Turk, 2004: Multivariate statisical integration of satellite infrared and microwave radiometric measurements for rainfall retrieval at the geostationary scale. *IEEE Transactions on Geoscience and Remote Sensing*, **42**(5), 1018–1032.

Robert, C.P. and G. Casella, 2004: Monte Carlo Statistical Methods. New York: Springer-Verlag.

Rosenfeld, D., D.B. Wolff, and E. Amitai, 1994: The window probability matching method for rainfall measurements with radar. *Journal of Apply Meteorology*, **33**, 683–693.

Rudolf, B., H. Hauschild, W. Rueth, and U. Schneider, 1994: Terrestrial precipitation analysis: operational method and required density of point measurements. Global Precipitations and

Climate Change, Edited by M. Desbois and F. Desalmand. NATO ASI Series, Vol. 1, No. 26, Berlin: Springer-Verlag, 173–186.

Seo, D.J. and J.P. Breidenbach, 2002: Real-time correction of spatially nonuniform bias in radar rainfall data using rain gauge measurements. *Journal of Hydrometeorology*, **3**(2), 93–111.

Simpson, J., R.F. Adler, G.R. North, 1988: A proposed Tropical Rainfall Measuring Mission (TRMM) satellite. *Bulletin of the American Meteorological Society*, **69**(3), 278–295.

Smith, J.A., and W.F. Krajewski, 1991: Estimation of the mean field bias of radar rainfall estimates. *Journal of Applied Meteorology*, **30**, 397–412.

Sorooshian, S., K.-L. Hsu, X. Gao, H.V. Gupta, B. Imam, and D. Braithwaite, 2000: Evaluation of PERSIANN system satellite-based estimates of tropical rainfall. *Bulletin of the American Meteorological Society*, **81**, 2035–2046.

Sorooshian, S., X. Gao, K. Hsu, R.A. Maddox, Y. Hong, B. Imam, and H.V. Gupta, 2002: Diurnal variability of tropical rainfall retrieved from combined GOES and TRMM satellite information. *Journal of Climate*, **15**, 983–1001.

Steiner, M., T.L. Bell, Y. Zhang, and E.F. Wood, 2003: Comparison of two methods for estimating the sampling-related uncertainty of satellite rainfall averages based on a large radar data set. *Journal of Climate*, **16**, 3759–3778.

Tapiador, F.J., C. Kidd, V. Levizzani, and F.S. Marzano, 2004a: A neural networks-based PMW-IR fusion technique to derive half hourly rainfall estimates at 0.1° resolution. *Journal of Applied Meteorology*, **43**, 576–594.

Tapiador, F.J., C. Kidd, K. Hsu, and F. Narzano, 2004b: Neural networks in satellite rainfall estimation. *Meteorolgocal Applications*, **11**, 83–91.

Turk, F.J., G. Rohaly, J.D. Hawkins, E.A. Smith, A. Grose, F.S. Marzano, A. Mugnai, and V. Levizzani, 2000: Analysis and assimilation of rainfall from blended SSM/I, TRMM and geostationary satellite data. Proc. 10th Conf. Satellite Meteorology and Oceanography, AMS, Long Beach, CA., 66–69.

Turk, F.J., P. Bauer, E. Ebert, and P. Arkin, 2006: Satellite-derived precipitation verification activities within the International Precipitation Working Group (IPWG). 14th Conference on Satellite Meteorology, Amer. Met. Soc, Washington, D.C., January 2006.

Vicente, G.A., R.A. Scofield, and W.P. Menzel, 1998: The operational GOES infrared rainfall estimation technique. *Bulletin of the American Meteorological Society*, **79**, 1883–1898.

Vincent, L. and P. Soille, 1991: Watersheds in digital spaces: an efficient algorithm based on immersion simulations. *IEEE Transactions on Pattern Analysis and Machine Intelligence*, **13**(6), 583–598.

Xie, P., and P.A. Arkin, 1995: An intercomparison of gauge observations and satellite estimates of monthly precipitation. *Journal of Applied Meteorology*, **34**, 1143–1160.

Xie, P., and P.A. Arkin, 1997: Global precipitation: a 17-year monthly analysis based on gauge observations, satellite estimates, and numerical model outputs. *Bulletin of the American Meteorological Society*, **78**, 2539–2558.

Xie, P., J.E. Janowiak, P.A. Arkin, R.F. Adler, A. Gruber, R. Ferraro, G.J. Huffman, and S. Curtis, 2003: GPCP pentad precipitation analyses: an experimental dataset based on gauge observations and satellite estimates. *Journal of Climate*, **16**, 2197–2214.

Xu, L., X. Gao, S. Sorooshian, P.A. Arkin, and B. Imam, 1999: A microwave infrared threshold technique to improve the GOES precipitation index. *Journal of Applied Meteorology*, **38**(5), 569–579.

Yi, H., 2002: Assimilation of satellite-derived precipitation into the regional atmospheric modeling system (RAMS) and its impact on the weather and hydrology in the southwest United States. Ph.D. dissertation, University of Arizona.

Yilmaz, K.K., T.S. Hogue, K. Hsu, S. Sorooshian, H.V. Gupta, and T. Wagener, 2005: Intercomparison of rain gauge, radar, and satellite-based precipitation estimates on hydrologic forecasting. *Journal of Hydrometeorology*, **6**(4), 497–517.